RESEARCH

Plasmonic Properties of Graphene Loaded Waveguide Bounded by Chiroferrite Medium

M. Shaban[1] · Zahraa J. Mohammed[2] · Hussein H. AbdulGhani[2] · Soror Ali Mahdi[3] · Hasan Majdi[4] · N. M. A. Hadia[5] · Laiba[6] · A. Waleed[7]

Abstract
Herein, plasmonic characteristics of graphene filled waveguide surrounded by chiroferrite medium are analyzed in the THz frequency spectrum. Graphene conductivity is modelled using the Kobo formula, and impedance boundary conditions are employed to compute dispersion relation. The influence of constitutive variables of chiroferrite medium on the propagation behavior of SPP mode is examined. The propagation behavior of SPPs mode is studied by changing the constitutive parameters of chiroferrite medium and graphene features. From numerical results, it is revealed that effective mode index (EMI, phase velocity, graphene conductivity, and EM wave frequency) can be tailored by adjusting chirality, gyrotropy, and graphene features (chemical potential, number of graphene layers) in the THz frequency range. This work may have potential applications in plasmonic community to design the innovative optical sensors, plasmonic platforms, detectors, and surface waveguides in the THz frequency region and provide active control due to additional degree of freedom in graphene and anisotropy of chiral medium.

Keywords SPPs · Graphene · Chiroferrite · Characteristics equation · Effective mode index · Phase velocity

Introduction

Over the last decade, surface plasmon polaritons (SPPs) have been the subject of research for their various unique features to design nanoscale electronic and photonic devices [1–8]. It is an emerging field of science and technology. Aside from sensing purposes [9–11], SPPs can also be used to control switches [12] and to build signal amplifiers and modulators [13–17]. In contrast to other conventional focusing techniques like dielectric lenses, a fundamental characteristic of SPPs is able to confining

✉ M. Shaban
mssfadel@aucegypt.edu

✉ Laiba
laiba222rana@gmail.com; physicsscholar232@gmail.com

Hussein H. AbdulGhani
100357@uotechnology.edu.iq

Soror Ali Mahdi
suroor.a.mahdi@uruk.edu.iq

Hasan Majdi
dr.hasanshker@mustaqbal-college.edu.iq

N. M. A. Hadia
nmhadia@ju.edu.sa

A. Waleed
ashanwaleed556@gmail.com

1   Department of Physics, Faculty of Science, Islamic University of Madinah, Madinah 42351, Saudi Arabia

2   Department of Applied Sciences, University of Technology, Baghdad, Iraq

3   Department of Medical Physics, College of Science, Uruk University, Baghdad, Iraq

4   Department of Chemical Engineering and Petroleum Industries, Al-Mustaqbal University College, Babylon 51001, Iraq

5   Physics Department, College of Science, Jouf University, Al-Jouf, P.O. Box 2014, Sakaka, Saudi Arabia

6   Department of Mathematics, Government College University, Faisalabad 38000, Pakistan

7   Department School of Energy Science and Engineering, Harbin Institute of Technology, Harbin 150001, China

electromagnetic fields to smaller scales, which distinguishes it from them [1, 18]. It is possible to greatly reduce the size of devices and systems by replacing free-space propagating electromagnetic (EM) waves with SPPs. When photons and electrons interact, the SPPs exhibit a larger wave vector than free space waves [19]. Metal-based structure plays an important role in determining the frequency range and propagation loss of SPPs modes [20]. Krokhin et al. studied the SPPs behavior in an anisotropic photonic crystal deposited on a thin metallic film to increase the efficiency of plasmonic devices [21]. Gric and Rafailov studied the SPPs propagation at metal free metamaterial with anisotropy of semiconductor to control the propagation length of SPPs [7]. Umair et al. presented the numerical analysis of plasmon modes in metallic filled parallel plate waveguide (PPWG) to investigate the effect of tensorial permittivity on the characteristics of EM surface wave [22]. Bousbih et al. studied the plasmon mode at chiroplasma-metal interface in the THz frequency regime [23]. Guangcan Mi and Vien Van studied the numerical investigation of SPPs at chiral-metal planar structure [24]. The propagation range of metallic based plasmonic structures is generally limited by Joule losses [21]. Additionally, the metal-based structures have a higher propagation loss, a lower tunability, and a lower confinement [25]. Currently, the plasmonic community is seeking 2D optical materials with low propagation losses. The introduction of graphene material is intended to address these bottleneck problems.

An atom-thick layer of carbon atoms known as graphene has recently attracted attention in the fields of plasmonic community [26, 27]. It has been demonstrated that graphene supports the surface plasmons in the mid-infrared (MIR) and terahertz (THz) ranges of the EM spectrum [28–32]. In comparison with noble metals, graphene has unique and remarkable optical properties including low losses, long propagation lengths, extreme confinement of light, and tunable conductivity [26, 28, 32]. Furthermore, the conductivity of graphene-based structures can be tuned much more easily than those of metallic and photonic crystal structures. Graphene's tunable conductivity allows the resonance characteristics to be altered without having to re-fabricate the device [33–36]. In graphene-based plasmonic devices, electrical gating is crucial for modulating the carrier concentration in the graphene layers, which alters graphene's electronic properties. As a result of this ability to control carrier concentration, graphene is an extremely versatile material for wide variety of technological applications, including transistors, sensors, and photonics [37]. Different authors used different geometries and different optical materials for the propagation of SPPs [24, 31, 38–43].

A substantial amount of literature has been devoted to electromagnetic propagation in chiral materials [44–47]. In the case of such an isotropic chiral material, the degree of chirality can be controlled only a limited extent once it has been created. Thus, it is imperative to develop methods for controlling chirality. The incorporation of certain forms of anisotropy enables the realization of such method. The composite chiroferrite material is made of isotropic chiral and a nonreciprocal ferrite material in which chiral material is encapsulated in a magnetically biased ferrite [48]. The permeability tensor can be modified by adjusting the tensor values, thereby controlling the chirality of SPPs waves at CF-G-CF interface.

Mathematical Formulation

Consider the propagation of SPPs in z direction as depicted in Fig. 1.

Here are the constitutive relationships for chiroferrite medium.

$$D = \varepsilon E + i\xi B \tag{1}$$

$$H = i\xi E + \overline{\mu}^{-1} B \tag{2}$$

$$\overline{\mu} = \begin{vmatrix} \mu_1 & -ik & 0 \\ ik & \mu_1 & 0 \\ 0 & 0 & \mu_3 \end{vmatrix} \tag{3}$$

In the chiroferrite medium:

$$E_z = A_1 e^{-q_1 x} + A_2 e^{-q_2 x} \tag{4}$$

$$H_z = i(A_1 \alpha_1 e^{-q_1 x} + A_2 \alpha_2 e^{-q_2 x}) \tag{5}$$

The rest of field components can be obtained from [49]. Based on the source-free Maxwell equations, coupled wave equations are presented below.

$$\nabla_t^2 E_z + P_1 E_z + iP2H_z = 0 \tag{6}$$

$$\nabla_t^2 H_z + iP_3 E_z + P4H_z = 0 \tag{7}$$

The coefficients for Eqs. 6 and 7 are

$$P_1 = \frac{\omega(d(\varepsilon_0 + \mu_z \xi^2) - \mu_z \xi b)}{D_2} \tag{8}$$

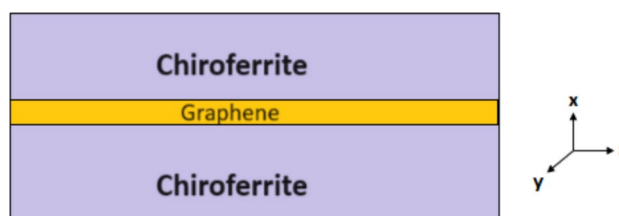$$P_2 = \frac{\omega \mu_z (b - d\xi)}{D_2} \tag{9}$$

Fig.1 Geometry for graphene loaded chiroferrite waveguide

$$P_3 = \frac{\omega(b(\varepsilon_0 + \mu_z \xi^2) + f0\mu_z\xi)}{D_2} \tag{10}$$

$$P_4 = \frac{\omega\mu_z(b\xi + f0)}{D_2} \tag{11}$$

where

$$a = \left[\beta^3 + 3\omega k\xi\beta^2 + 2\omega^2\xi^2\beta(\mu_1^2 - k^2) + \omega^2\mu_1\varepsilon_0\beta\right]/D_1 \tag{12}$$

$$b = \left[\omega\beta(\mu_1\xi\beta + \omega\varepsilon_0 k) + \omega^3\varepsilon_0\xi(\mu_1^2 - k^2)\right]/D_1 \tag{13}$$

$$c = \left[2\omega^2\xi\beta(\mu_1^2 - k^2) + \omega k\beta^2\right]/D_1 \tag{14}$$

$$d = \left[-\omega\mu_1\beta^2 - \omega^3\varepsilon_0(\mu_1^2 - k^2)\right]/D_1 \tag{15}$$

$$e = -\omega\left[\xi\beta(2\omega\varepsilon_0\mu_1 + \xi k\beta) + 2\omega\xi^3\beta(\mu_1^2 - k^2) + \omega^2\varepsilon_0^2 k\right]/D_1 \tag{16}$$

$$f0 = \left[\omega\beta^2(\varepsilon_0 + \mu_1\xi^2) - 2\omega^2\varepsilon_0\xi c\beta k - \omega^3\xi c^2\varepsilon_0(\mu_1^2 - k^2) - \omega^3\varepsilon_0^2\mu_1\right]/D_1 \tag{17}$$

$$D_1 = \beta^4 + 4\omega^2\xi^2\beta^2(k^2 - \mu_1^2) - 2\omega^2\beta^2\mu_1\varepsilon_0 + \omega^4\varepsilon_0^2(\mu_1^2 - k^2) - 4\omega\xi\beta^3 k \tag{18}$$

$$D_2 = b^2 + df \tag{19}$$

$$q_1 = \sqrt{\frac{P_1 + P_4 + \sqrt{(P_1 - P_4)^2 - 4P_2 P_3}}{2}} \tag{20}$$

$$q_2 = \sqrt{\frac{P_1 + P_4 - \sqrt{(P_1 - P_4)^2 - 4P_2 P_3}}{2}} \tag{21}$$

$$\alpha_1 = \frac{P_1 - (q_1)^2}{P_2} \tag{22}$$

$$\alpha_2 = \frac{P_1 - (q_2)^2}{P_2} \tag{23}$$

$$\hat{x} \times [H_1 - H_2] = \sigma E \tag{24}$$

$$\hat{x} \times [E_1 - E_2] = 0 \tag{25}$$

The conductivity of graphene is described as follows:

$$\sigma = \frac{je^2(\omega - j\tau^{-1})}{\pi h^2} \times \left[\frac{1}{(\omega - j\tau^{-1})^2}\int_0^\infty \times \xi\left(\frac{\sigma f_d(\xi, \mu_c, T)}{\sigma\xi} - \frac{\sigma f_d(-\xi, \mu_c, T)}{\sigma\xi}\right)d\xi - \int_0^\infty \times \frac{f_d(-\xi, \mu_c, T) - f_d(\xi, \mu_c, T)}{(\omega - j\tau^{-1})^2 - 4(\xi/\hbar)^2}d\xi\right] \tag{26}$$

Using Eqs. 26 and 27, the following characteristic is obtained:

$$i\sigma q_1(b - d\alpha_1) + q_2(-ib\sigma + \alpha_2(id\sigma + 2(b^2 + df0)q_1)) - 2(b^2 + df0)q_1\alpha_1 = 0 \tag{27}$$

Numerical Results

In this section, numerical results have been carried out to obtain the deeper understanding the features of SPPs at the CF-G-CF planar interface. Combining both optical materials, i.e., (graphene and chiroferrite), enables us to gain a deeper understanding of the engineerable properties of SPPs. Monolayer graphene is sandwiched between chiroferrite layers as depicted in Fig. 1. To understand the plasmonic features of plasmon mode at a CF-G-CF interface, dispersion relation is plotted between EMI and wave frequency in THz regime under the different graphene as well as chiroferrite parameters. In this context, Maxwell's equations for planar structure are used to derive the dispersion relation. In our calculation, we have set numerical parameters as μ_c=0.5 eV, $T = 300K$, $\xi_c = 0.2$, $\tau = 12ps$, and $\mu_2 = 0.52\mu_0$. The EMI spectra for different magnitude of graphene's chemical potential and graphene layers are displayed in Fig. 2a and b, respectively. According to Fig. 2a, to achieve the plasmonic properties, chemical potential extends from $\mu_c = 0.3eV$ to $\mu_c = 0.6eV$ indicated by black, green, red, and blue peaks. The rise in chemical potential shifts the characteristics peaks towards higher frequency spectrum. In addition, as chemical potential increases, the frequency band starts to narrow. The squeezing of the frequency band gap with an increasing amount of chemical potential provides an additional degree of freedom for modulating EM surface waves. Moreover, lower chemical potential leads to higher EMI as reported [6, 43, 50, 51]. Because when the concentration of graphene carriers is low enough, both the valence band and the conduction band overlap at the Dirac point in the Brillouin zone. Upon reaching this point, the relationship between energy and momentum becomes linear, resulting in distinct electronic properties for plasmonic community. Linear dispersion is a key component of nanoscale devices that facilitates strong coupling between light and matter, as well as efficient energy transfer. The carrier concentration of graphene can be modified by electrostatic gating or chemical doping [31, 42, 52], thereby allowing dynamic control of plasmon response enabled the advanced technological applications

Fig. 2 The influence of chemical potential and number of graphene layers on EMI versus EM wave frequency
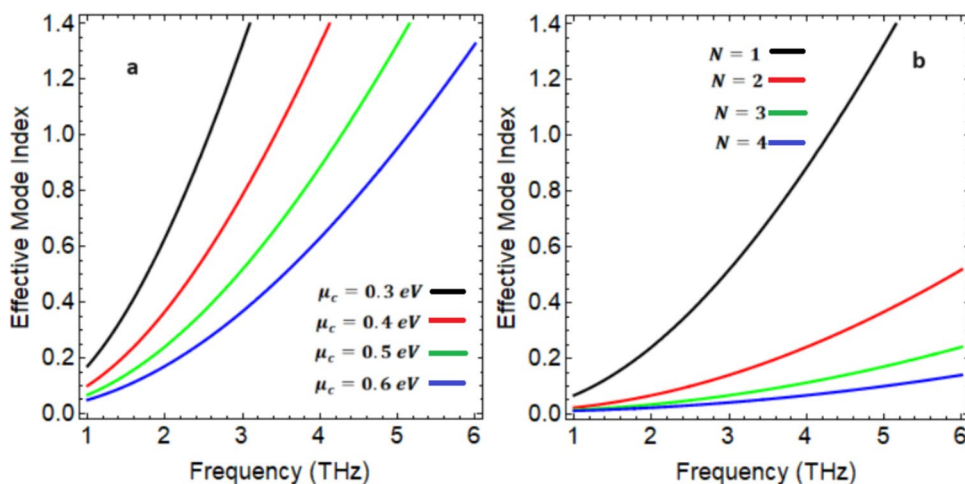
for plasmonic sector. Figure 2b illustrates the EMI under different graphene layers. According to a recent study, only 2.3% of the incident light is absorbed by single layer of graphene [37, 53]. It can be noted that EMI reduces with the number of layers of graphene. Based on the numerical analysis, it is clearly manifest that single-layer graphene ($N = 1$) exhibits lower energy losses than multilayered graphene as reported in [53–56]. Furthermore, numerical analysis shows that multilayer graphene causes to shifts the characteristic peak toward the high frequency region. The influence of chirality on EMI is graphically depicted in Fig. 3a under different chirality range $\xi_c = 0.2$, $\xi_c = 0.3$, $\xi_c = 0.4$, and $\xi_c = 0.5$. Figure 3a illustrates how EMI decreases with the increment of chirality parameter. As chirality increases, wave frequency decreases, and dispersion curves reflect lower EMI [23]. Thus, the frequency and EMI of the CF-G-CF structure can be controlled by adjusting the chirality values. It is of peculiar of interest to note that the slope of dispersion curve is smaller for higher chirality values. To illustrate the effect of gyrotropy on the behavior of SPPs, Fig. 4b illustrates the influence

of gyrotropy on EMI as a function of wave frequency. It is obvious that as gyrotropy increases, frequency band broadened, and dispersion curves reflect higher EMI. Recently, Razzaz et al. presented the numerical analysis of EM surface wave in graphene filled waveguide bounded by magnetic material [56]. In our proposed structure, the introduction of chirality in the ferrite medium provides an additional degree of freedom. It is important to note that when a wave interacts with a gyrotropic medium, its velocity is altered, affecting its speed of propagation. Changing the direction of the polarization plane reduces propagation losses and allows the wave to interact more effectively with the material. These extraordinary features of ferrite mediums with increased gyrotropy are widely used in optics community to fabricate nano plasmonic devices. The choice of an appropriate gyrotropy of medium is crucial for the design of nanophotonic devices based on chiroferrite-graphene in a specific frequency band. Figure 4a depicts the effects of chemical potential on phase velocity. As chemical potential increases, the dispersion curves shift from low to high frequency region. Thus, it is concluded

Fig. 3 The influence of chirality and gyrotropy on EMI versus EM wave frequency
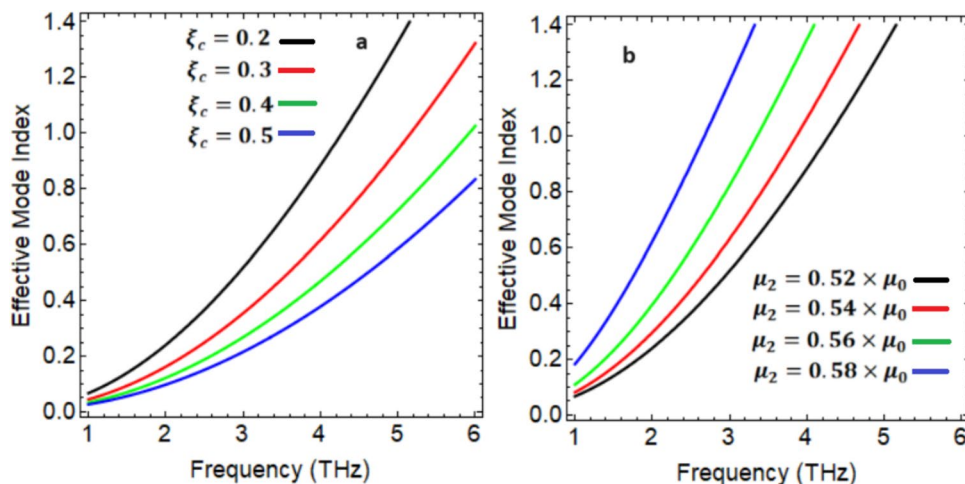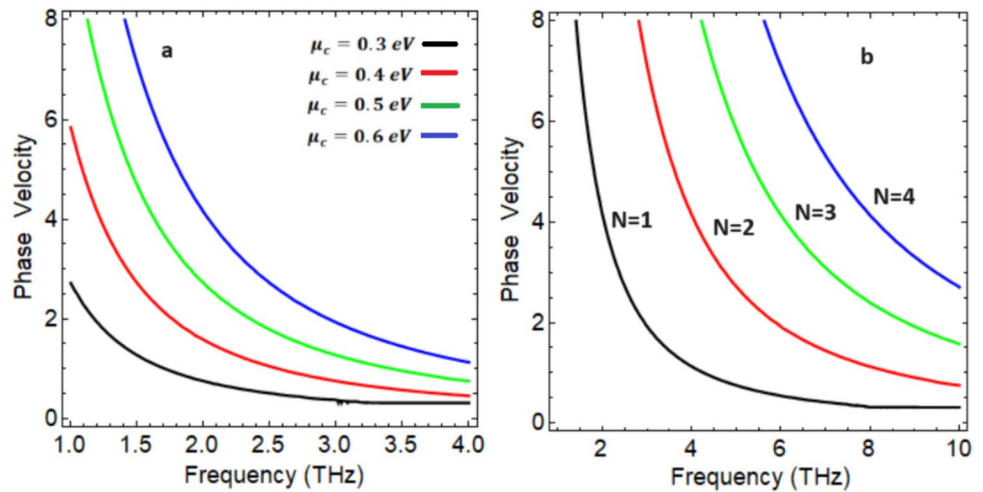
Fig. 4 The impact of chemical potential and number of graphene layers on phase velocity versus EM wave frequency

that the phase velocity and frequency band of the proposed structure can be adjusted through the tuning of graphene's chemical potential. The effect of number of graphene layers on phase velocity of EM surface waves with respect to EM frequency is graphically demonstrated in Fig. 4b. It is observed that multilayer graphene support high frequency as compared with monolayer graphene. To analyze, the variation in phase velocity for different values of chirality and gyrotropy is shown in Fig. 5a and b, respectively. Figure 5a illustrates how phase velocity varies with chirality. Obviously, as magnitude of chirality increases, EM waves frequency increases and bandgap starts squeezing. Furthermore, it is of peculiar of interest to note that highest slope of variation is observed for lowest chirality value, i.e., $\xi_c = 0.2$. In Fig. 5b, we demonstrate the impact of varying gyrotropy of chiroferrite medium on the phase velocity. In this regard, frequency range is taken from 1 to 6 THz. As gyrotropy increase, the EM wave frequency decreases, but bandgap becomes broadened. Figure 6a and

b describes the impact of chemical potential and EM wave frequency on EMI versus graphene conductivity, respectively, by using dispersion relation 27. It is possible to tune the chemical potential of a compound by doping it or applying external fields to it as reported in [39, 41, 42]. According to Fig. 6a, as chemical potential rises, graphene conductivity decreases. It is important to note that graphene's carrier density increases in proportion to its chemical potential. Increasing carrier density may result in more scattering events. As a result of these scattering events, charge carriers have a lower mobility, which results in a lower conductivity.

Impact of different EM wave frequencies on EMI versus graphene conductivity is presented in Fig. 6b. It is clearly manifest that as EM wave frequency increases, graphene conductivity decreases. Increasing EM wave frequency hinders the dynamic response of charge carriers, increases scattering, and causes energy to be absorbed by interband transitions and other processes, reducing graphene's conductivity.

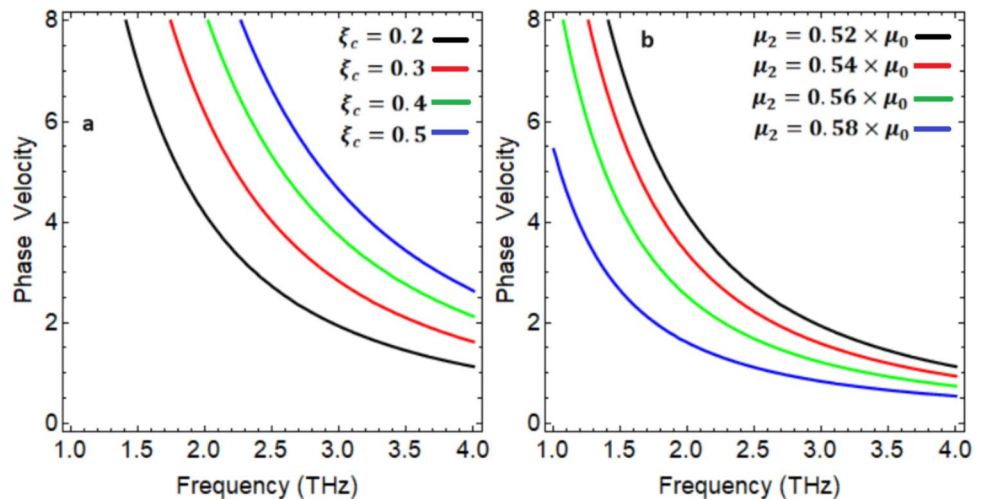**Fig. 5** The impact of chirality and gyrotropy on phase velocity versus EM wave frequency

Fig. 6 The influence of chemical potential and EM wave frequency on EMI versus graphene conductivity
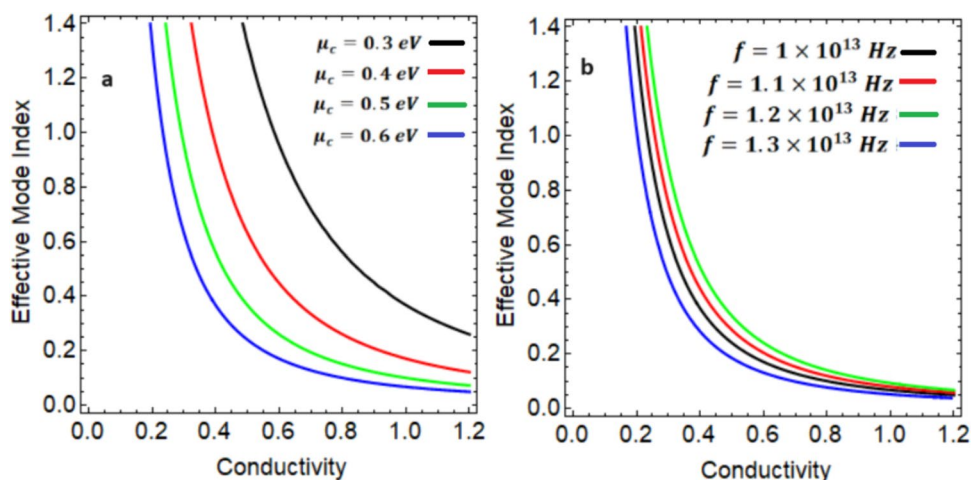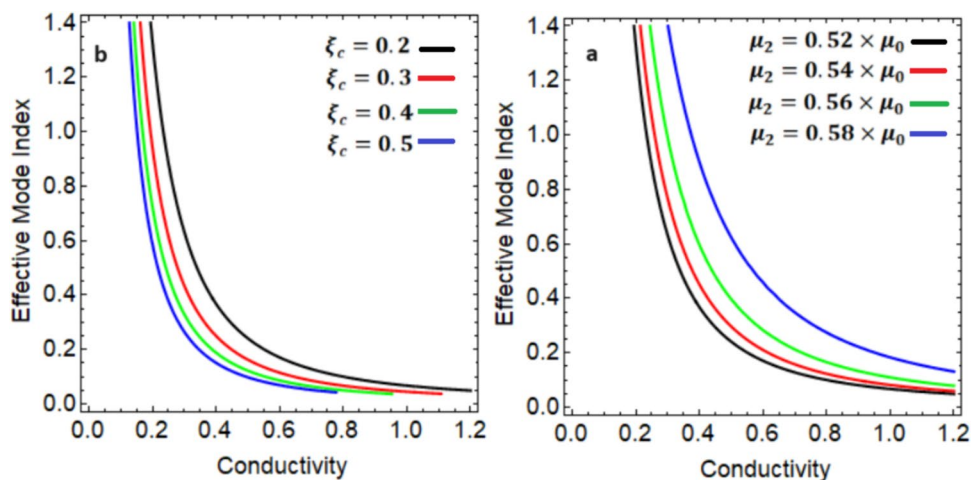

Fig. 7 The influence of chirality and gyrotropy on EMI versus graphene conductivity

The effect of chirality and gyrotropy on EMI versus graphene conductivity by using dispersion relation 27. The influence of chirality on EMI versus graphene conductivity is plotted in Fig. 7a. Clearly, the conductivity of graphene decreases with increasing chirality. Furthermore, slope of dispersion curve is smaller for higher chirality value. It is important to note that graphene's electronic properties are highly dependent on its surroundings medium. The effect of gyrotropy on EMI versus graphene conductivity is shown in Fig. 7b. As gyrotropy of chiroferrite medium increases, the dispersion curves shifted towards higher conductivity. Since, gyrotropic nature of the chiroferrite medium generates magneto-optical effects, such as the Faraday effect, which causes light's polarization plane to rotate. As a result of these effects, the charge carriers in graphene are aligned, resulting in reduced resistive losses and increased graphene conductivity.

Concluding Remarks

This study focuses on the features of electromagnetic surface waves generation at the CF-G-CF planar interface. It is demonstrated that the propagation characteristics associated with surface waves are strongly influenced by the chiroferrite and graphene parameters. These characteristics of the CF-G-CF structure are EMI, phase velocity, and characteristics curve. Additionally, frequency fluctuations offer flexibility in modifying and altering the propagation of surface waves for the proposed structure. The calculated numerical results of this research work may be useful in plasmonic community to design the innovative optical sensors, plasmonic platforms, detectors, and surface waveguides in the THz frequency region and provide active control due to additional degree of freedom in graphene and anisotropy of chiral medium.

Author Contribution The author confirms their contribution to the manuscript as follows: M. Shaban and Laiba wrote the main manuscript. Zahraa J. Mohammed, Hussein H.AbdulGhani, Soror Ali Mahdi, Hasan Majdi derived the methodology section. N.M.A Hadia, Laiba, A. Waleed wrote result and discussion section. M. Shaban and Laiba were also encouraged and completely supervised during preparation of the manuscript. All authors reviewed the manuscript before submission.

Data Availability Detail about data has been provided in the article.

Declarations

Ethical Approval Not applicable.

Competing Interests The authors declare no competing interests.

References

1. Barnes WL, Dereux A, Ebbesen TW (2003) Surface plasmon subwavelength optics. Nature 424(6950):824–830

2. Gramotnev DK, Bozhevolnyi SI (2010) Plasmonics beyond the diffraction limit. Nat Photonics 4(2):83–91

3. Umair M et al (2023) Light plasmon coupling in planar chiroplasma–graphene waveguides. Plasmonics 18(3):1029–1035

4. Umair M et al (2024) Plasmonic characteristics of monolayer graphene in anisotropic plasma dielectric. Plasmonics 19(3):1165–1171

5. Umair M, Ghaffar A, Razzaz F, Saeed SM (2023) Hybrid plasmon modes at chiroferrite-graphene interface. Plasmonics 1–7

6. Gric T, Hess O (2017) Tunable surface waves at the interface separating different graphene-dielectric composite hyperbolic metamaterials. Opt Express 25(10):11466–11476

7. Gric T, Rafailov E (2022) Propagation of surface plasmon polaritons at the interface of metal-free metamaterial with anisotropic semiconductor inclusions. Optik 254:168678

8. Nickelson L et al (2008) Electrodynamical analyses of dielectric and metamaterial hollow-core cylindrical waveguides. Elektronika ir elektrotechnika 82(2):3–8

9. Hutter E, Fendler JH (2004) Exploitation of localized surface plasmon resonance. Adv Mater 16(19):1685–1706

10. Raschke G et al (2003) Biomolecular recognition based on single gold nanoparticle light scattering. Nano Lett 3(7):935–938

11. Yonzon CR et al (2004) A comparative analysis of localized and propagating surface plasmon resonance sensors: The binding of concanavalin A to a monosaccharide functionalized self-assembled monolayer. J Am Chem Soc 126(39):12669–12676

12. Umair M, Ghaffar A, Alkanhal MA, Khan Y, Shahid MU (2024) Tunability of plasmon modes at uniaxial chiral–black phosphorus planar structure. Plasmonics 1–9

13. Hoekstra H et al (1998) A cost 240 benchmark test for beam propagation methods applied to an electrooptical modulator based on surface plasmons. J Lightwave Technol 16(10):1921

14. Jung C, Yee S, Kuhn K (1994) Integrated optics waveguide modulator based on surface plasmon resonance. J Lightwave Technol 12(10):1802–1806

15. Krasavin A et al (2004) High-contrast modulation of light with light by control of surface plasmon polariton wave coupling. Appl Phys Lett 85(16):3369–3371

16. Nikolajsen T, Leosson K, Bozhevolnyi SI (2004) Surface plasmon polariton based modulators and switches operating at telecom wavelengths. Appl Phys Lett 85(24):5833–5835

17. Sasaki K, Nagamura T (1998) Ultrafast wide range all-optical switch using complex refractive-index changes in a composite film of silver and polymer containing photochromic dye. J Appl Phys 83(6):2894–2900

18. Yin L et al (2005) Subwavelength focusing and guiding of surface plasmons. Nano Lett 5(7):1399–1402

19. Zhang X et al (2020) Terahertz surface plasmonic waves: A review. Adv Photonics 2(1):014001–014001

20. Zhou F et al (2017) Extending the frequency range of surface plasmon polariton mode with meta-material. Nano-Micro Letters 9:1–8

21. Krokhin AA, Neogi A, McNeil D (2007) Long-range propagation of surface plasmons in a thin metallic film deposited on an anisotropic photonic crystal. Phys Rev B 75(23):235420

22. Umair M et al (2023) Plasmonic modes of metallic slab in anisotropic plasma environment. Plasmonics 18(5):1857–1864

23. Bousbih R, Soliman MS, Jafar NN, Jabir MS, Majdi H, Alshomrany AS, Hadia NM, Shaban M, El-Badry YA, Iftikhar M (2024) Generation of surface plasmon polaritons (SPPs) at chiroplasma-metal interface. Plasmonics 1–6

24. Mi G, Van V (2014) Characteristics of surface plasmon polaritons at a chiral–metal interface. Opt Lett 39(7):2028–2031

25. Azam M, Umair M, Ghaffar A, Alkanhal MA, Alqahtani AH, Khan Y (2024) Dispersion characteristics of surface plasmon polaritons (SPPs) in graphene–chiral–graphene waveguide. Waves Random Complex Media 34(1):134–145

26. Bonaccorso F et al (2010) Graphene photonics and optoelectronics. Nat Photonics 4(9):611–622

27. Shokati E, Granpayeh N, Danaeifar M (2017) Wideband and multi-frequency infrared cloaking of spherical objects by using the graphene-based metasurface. Appl Opt 56(11):3053–3058

28. Garcia de Abajo FJ (2014) Graphene plasmonics: challenges and opportunities. ACS Photonics 1(3):135–152

29. Asgari S, Shokati E, Granpayeh N (2019) High-efficiency tunable plasmonically induced transparency-like effect in metasurfaces composed of graphene nano-rings and ribbon arrays and its application. Appl Opt 58(13):3664–3670

30. Hanson GW (2008) Dyadic green's functions and guided surface waves for a surface conductivity model of graphene. J Appl Phys 103(6)

31. Saeed M et al (2021) Hybrid energy surface plasmon modes supported by graphene-coated circular chirowaveguide. Opt Mater 114:110869

32. Asgari S et al (2018) Tunable graphene-based mid-infrared band-pass planar filter and its application. Chin Phys B 27(8):084212

33. Chen Y, Wang W, Zhu Q (2014) Theoretical study on biosensing characteristics of heterostructure photonic crystal ring resonator. Optik 125(15):3931–3934

34. Goldflam MD et al (2017) Designing graphene absorption in a multispectral plasmon-enhanced infrared detector. Opt Express 25(11):12400–12408

35. Li H-J et al (2014) Controlling mid-infrared surface plasmon polaritons in the parallel graphene pair. Appl Phys Express 7(12):125101

36. Meng H et al (2017) Tunable graphene-based plasmonic multispectral and narrowband perfect metamaterial absorbers at the mid-infrared region. Appl Opt 56(21):6022–6027

37. Saeed M et al (2022) Graphene-based plasmonic waveguides: a mini review. Plasmonics 17(3):901–911

38. Heydari MB, Samiei MH (2021) Chiral multi-layer waveguides incorporating graphene sheets: an analytical approach. arXiv preprint arXiv:2102.10135

39. Heydari MB, Vadjed Samiei MH (2020) Analytical study of hybrid surface plasmon polaritons in a grounded chiral slab waveguide covered with graphene sheet. Opt Quantum Electron 52(9):406

40. Iftikhar M, Raza A, Alkhouri A, Ibrahim SH, Obaidullah AJ, Mahal A, Hamza M (2024) Numerical investigations of SPPs at chiroferrite-metal interface. Plasmonics 1–6

41. Saeed M et al (2021) Characteristics of hybrid surface plasmon polaritons at a chiral graphene metal interface in cylindrical waveguides. Opt Quant Electron 53:1–14

42. Yaqoob M et al (2018) Hybrid surface plasmon polariton wave generation and modulation by chiral-graphene-metal (CGM) structure. Sci Rep 8(1):18029

43. Yaqoob MZ et al (2019) Characteristics of light–plasmon coupling on chiral–graphene interface. JOSA B 36(1):90–95

44. Engheta N, Pelet P (1989) Modes in chirowaveguides. Opt Lett 14(11):593–595

45. Hui H-T, Yung A (1996) The eigenfunction expansion of dyadic Green's functions for chirowaveguides. IEEE Trans Microw Theory Tech 44(9):1575–1583

46. Svedin JA (1990) Propagation analysis of chirowaveguides using the finite-element method. IEEE Trans Microw Theory Tech 38(10):1488–1496

47. Umair M et al (2021) Dispersion characteristics of hybrid surface waves at chiral-plasma interface. J Electromagn Waves Appl 35(2):150–162

48. Xu J et al (2009) Electromagnetic wave propagation in an elliptical chiroferrite waveguide. J Electromagn Waves Appl 23(14–15):2021–2030

49. Gong J (1999) Electromagnetic wave propagation in a chiro-plasma-filled waveguide. J Plasma Phys 62(1):87–94

50. Gric T (2019) Tunable terahertz structure based on graphene hyperbolic metamaterials. Opt Quant Electron 51(6):202

51. Heydari MB, Samiei MHV (2021) TM-polarized surface plasmon polaritons in nonlinear multi-layer graphene-based waveguides: an analytical study. arXiv preprint arXiv:2101.02536

52. Efetov DK, Kim P (2010) Controlling electron-phonon interactions in graphene at ultrahigh carrier densities. Phys Rev Lett 105(25):256805

53. Azam M et al (2021) Dispersion characteristics of surface plasmon polaritons (SPPs) in graphene–chiral–graphene waveguide. Waves Random Complex Media 1–12

54. Shahid MU, Ghaffar A, Naz MY, Bhatti HN (2023) Electromagnetic waves in graphene-coated partially filled chiroplasma cylindrical waveguide. Plasmonics 18(5):1979–1989

55. Umair M et al (2020) Characteristics of surface plasmon polaritons in magnetized plasma film walled by two graphene layers. J Nanoelectron Optoelectron 15(5):574–579

56. Razzaz F, Nawaz A, Ghaffar A (2024) Tunable properties of graphene loaded waveguide surrounded by magnetic materials. Digest J Nanomater Biostruct 19(1)